*Psychophysiology, 49* (2012), 1454–1463. Wiley Periodicals, Inc. Printed in the USA.

DOI: 10.1111/j.1469-8986.2012.01458.x

# Common N1 and mismatch negativity neural evoked components are revealed by independent component model-based clustering analysis

DIEGO LOZANO-SOLDEVILLA,[a,b] JOSEP MARCO-PALLARÉS,[c,d] LLUÍS FUENTEMILLA,[d] AND CARLES GRAU[a]

[a]Psychiatry and Clinical Psychobiology Department, University of Barcelona, Barcelona, Spain
[b]Radboud University Nijmegen, Donders Institute for Brain, Cognition and Behaviour, Nijmegen, The Netherlands
[c]Basic Psychology Department, University of Barcelona, Barcelona, Spain
[d]Cognition and Brain Plasticity Group, Bellvitge Biomedical Research Institute (IDIBELL), Barcelona, Spain

**Abstract**

Mismatch negativity (MMN) is an event-related brain potential that appears when an auditory regularity is violated. Two main hypotheses have been proposed to explain it: the adaptation hypothesis and the memory-based hypothesis. Critically, they differ in whether the MMN can be distinguished from the N1. In this study, we assessed the differential contribution of the N1 and the MMN using independent component analysis (ICA) combined with model-based clustering. Our results show that the neural responses associated with the standard and deviant tones are explained by three clusters of reliable ICs with frontocentral scalp distribution. Two of these clusters exhibited a common N1 for both the standard and deviant tones and one cluster showed an enhancement of the anterior N1 at the MMN time range. These results support the adaptation hypothesis, which proposes that MMN is generated by neural mechanisms similar to those associated with auditory N1.

**Descriptors:** Independent component analysis, Mismatch negativity, N1

To survive in potentially hostile environments, animals need to automatically detect changes in a uniform background to determine their nature and, if needed, act to prevent undesirable consequences. Significant advances in the study of brain activity related to the violation of regularities in auditory stream patterns have been made in the past few decades. It is well-established that the N1 component peaks approximately 100 ms after the onset of simple auditory stimuli (Näätänen & Picton, 1987). However, when a rare (deviant) sound is embedded into a sequence of regular (standard) tones, it evokes an enhanced frontocentral negative potential in the 120–250 poststimulus latency range referred to as mismatch negativity (MMN; Näätänen, Gaillard, & Mäntysalo, 1978; Näätänen, Paavilainen, Rinne, & Alho, 2007). It is generally accepted that MMN represents a very early (if not the earliest) automatic index of the auditory change detection process; as such, it has been studied extensively in many experimental settings (Näätänen et al., 1978, 2007). However, the neural mechanisms and the idiosyncrasy underlying MMN generation remain a matter of debate (Garrido, Kilner, Stephan, & Friston, 2009). At the poles of this debate, two explanatory models have been proposed: the memory-based model and the adaptation model.

The *memory-based model* holds that MMN appears as a consequence of a breakdown of earned auditory stream regularity because current auditory input is compared to a formed memory trace that is built up as sensory-memory representations that encode repetitive aspects of the auditory environment (Näätänen, 1992; Näätänen & Winkler, 1999). This model assumes that the MMN reflects the activity of specific groups of auditory neurons that transiently signal that there is an incoming sound that does not fit the previously repeated auditory pattern of stimulation. The neural population responsible for detecting a change in incoming sound would be different from the set of neurons that respond to previously repeated sound input. Consequently, the model states that the functional distinction between the N1 and MMN stems from the premise that the MMN (derived by subtraction) should be treated as an event-related fields/event-related potentials (ERF/ERP) component independent from the N1 (one element of the subtraction), so that the response to the deviance is the linear sum of the N1 and the MMN. In contrast, the *adaptation model* suggests that in each stimulus (or pattern) repetition of the conditions of

The authors would like to thank David M. Groppe for sharing the code of the split-half reliability analysis and for his help on script assessment and data analysis. We also thank Filipa Campos-Viola for solving our software bugs with the CORRMAP plug-in and Arnaud Delorme, Scott Makeig, and Wendy Martinez for their generous gift of software (EEGLAB and EDA Toolbox). This study was supported by grants from the Generalitat de Catalunya (SGR2009-00093), the Ministerio de Ciencia y Tecnología (SEJ2006-13998 to CG, PSI2009-09101 to JMP, and PSI2010-15024 to LlF), the Ramón y Cajal program (RYC-2007-01614 to JMP and RYC-2009-05471 to LlF), and the Fundació la Marató (2006-061632 to CG and JMP).

Address correspondence to: Josep Marco-Pallarés, Ph.D., Basic Psychology Department, Campus Bellvitge, University of Barcelona, 4a planta del Pavelló de Govern, Feixa Llarga s/n,08907 L'Hospitalet (Barcelona), Spain. E-mail: josepmarco@gmail.com



PSYCHOPHYSIOLOGY

stimulation, neurons of the auditory cortex become attenuated by a combination of the poststimulus suppressive mechanisms of adaptation and lateral inhibition (May et al., 1999; May & Tiitinen, 2010) and, as a consequence, there is a reduction (suppression) of the N1 amplitude with the repetition (Grau, Fuentemilla, & Marco-Pallarés, 2007). The key proposal of the adaptation hypothesis is the differential behavior of adapted and nonadapted neural responses. When a deviant sound is embedded in a set of regular tones, the nonadapted cells ("the fresh afferents") fire, contributing to an enhanced N1. In this model, the standard and the unexpected stimuli would activate, within the same brain region (i.e., the auditory cortex), different neural populations: while in response to the former neural responses, leading to an adapted state (adapted cells), the "fresh afferents" nonadapted cells would fire to the new/changed characteristics of the unexpected stimulus. Therefore, as stated in May and Tiitinen (2010), "The same areas partake in generating the N1 to the standard and the enhanced response to the deviant, and, consequently, there is no separate cortical area generating the MMN component" (pp. 71).

Several attempts have been performed to test both theories. Whether the MMN is generated from a different auditory neural population (i.e., the memory-based model) or, instead, from the same neural population that elicited the N1 ERP (i.e., the adaptation-based model) represents the critical cutting point between both models. The study of the temporospatial scalp distribution of the MMN and N1 might be conceived as an important approach that may help in disambiguating between the two generation proposals. For instance, finding differences at the spatial and temporal domain between the MMN and N1 would support the memory-based model (Näätänen, Jacobsen, & Winkler, 2005). Indeed, while the N1 topography is larger in the contralateral hemisphere after stimulation, the MMN presents a consistent right lateralization in response to simple sounds independent from the side of stimulation (Alain, Woods, & Ogawa, 1994; Giard, Perrin, Pernier, & Bouchet, 1990; Paavilainen, Alho, Reinikainen, Sams, & Näätänen, 1991, but see also Deouell, Bentin, & Giard, 1998). In addition, magnetoencephalographic (MEG) source localization studies have proposed that generators of N1 and MMN are separated by ~10 mm, suggesting that there is a specific neural network involved in MMN (Alho, 1995; Alho et al., 1998). Using the same line of reasoning, the latencies of N1 and MMN are very different, the former peaking at ~85 ms after the presentation of the stimuli and the latter at ~150 ms after the appearance of a deviant sound (Jääskeläinen et al., 2004; Näätänen & Picton, 1987). Other experiments demonstrate that MMN is elicited when detecting changes in complex auditory patterns. For example, MMN can appear when a sound is omitted in a regular auditory pattern (Tervaniemi, Saarinen, Paavilainen, Danilova, & Näätänen, 1994; Yabe, Tervaniemi, Reinikainen, & Näätänen, 1997). As it would appear obvious that omission would never generate an N1 ERP, the presence of MMN in this condition would support the presence of an independent mechanism of change detection. In addition, MMN also appears in abstract changes, such as in the violation of regular changes in frequency (Tervaniemi et al., 1994) or in the relationship between intensity and frequency (Paavilainen, Simola, Jaramillo, Näätänen, & Winkler, 2001). According to the memory-based model, this abstract-detection mechanism is an index of a primitive intelligence (Näätänen, Tervaniemi, Sussman, Paavilainen, & Winkler, 2001), which cannot be explained by means of an adaptation process, as sounds are not repeated and violations occur at the abstract level.

Nevertheless, the study of the spatiotemporal properties of the appearance of the N1 and MMN has also lent important support to the adaptation-based model. Jääskeläinen et al. (2004) showed, in a combined magnetoencephalography (M/EEG) and fMRI study, that the N1 and MMN had common source auditory neural population origins and that the delayed peak latency of the MMN could be explained by the alteration of the "center of gravity" of the activity within this neural population, being more anterior for MMN and more posterior for N1 (Jääskeläinen et al., 2004). Furthermore, the neurophysiological premises underlying the adaptation model are based on several physiological studies that showed adaptation and lateral inhibition in the auditory cortex, while studies showing cell populations that specifically fire in response to auditory change but not in response to standard tones are rare and controversial (Kropotov et al., 2000; May & Tiitinen, 2010). Jääskeläinen and colleagues also showed that an MMN was not generated by a separate group of neurons when compared to areas involved in single-sound processing (Jääskeläinen et al., 2004). This would argue against the existence of groups of neurons that specialize in auditory change detection. Finally, in a very exhaustive review, May and Tiitinen exposed, through computational simulations, that the adaptation model might account for most of the results found in the literature, including those that have been proposed to demonstrate the memory-based model, such as the elicitation of an MMN by stimulus omission or abstract changes (May & Tiitinen, 2010). In addition, Occam's razor would favor its validity, as the adaptation model is simpler and more physiologically based than the traditional model.

Furthermore, one of the primary criticisms of the conclusions derived from the memory-based model is centered in the rationale of using a subtraction method when identifying the MMN. In practically all MMN studies, the N1 response to the standard tone is subtracted from the response to the deviant tone, and the resulting subtraction curve is treated as a separate component, that is, a "genuine" brain response reflecting the activity arising out of a dedicated neural generator. Although the subtraction procedure may be intuitively valid when a priori assuming that the N1 and MMN are generated separately, this procedure may underestimate the possibility that they were elicited by common neurophysiological mechanisms with an unfixed response latency (May & Tiitinen, 2010). Indeed, in the adaptation model, the adapted and nonadapted neural activity that elicits the N1 ERP presents not only different amplitudes but different temporal dynamics. The N1 ERP that originates from adapted neural activity might peak earlier than the N1 that is primarily contributed by nonadapted neural responses. Therefore, the study of the temporal dynamics of N1/MMN might convey critical information regarding the nature of the neural generators that contribute to their appearance. Hence, a method that takes into consideration the temporal information when extracting functionally dissociated neural components seems, at first glance, appropriate here. Independent component analysis (ICA) represents a blind source-separation technique that decomposes a mixture of signals (EEG data, in our case) into their maximal independent components (IC) based on temporal information (Makeig, Bell, Jung, & Sejnowski, 1996; Makeig, Debener, Onton, & Delorme, 2004). It has been shown that ICA is able to separate ocular and muscular artifacts in EEG and MEG signals (Jung et al., 2000, 2001) and to identify spatiotemporal event-related brain responses (see, among others, Debener, Makeig, Delorme, & Engel, 2005; Delorme, Westerfield, & Makeig, 2007; Grau et al., 2007; Kalyakin, González, Kärkkäinen, & Lyytinen,

2008; Makeig et al., 1996; Makeig, Jung, Bell, Ghahremani, & Sejnowski, 1997; Marco-Pallarés, Grau, & Ruffini, 2005; Onton, Delorme, & Makeig, 2005). In the present study, we aimed to investigate whether MMN and N1 ERPs arise as a single or a dissociated component that is detectable in scalp electroencephalographic data (EEG) with a new single trial-based statistical approach based on ICA.

However, there are some shortcomings with regards to the use of ICA; namely, ICA might not be reliable when inadequate data (i.e., noise) are provided or when there are multiple local minima in the algorithm's objective function (Groppe, Makeig, & Kutas, 2009). Furthermore, after applying single-subject ICA, a cross-participant IC comparison procedure is needed to identify representative ICs between participants under specific experimental conditions. Indeed, clustering approaches have emerged as a successful way to address this methodological drawback. Different algorithms, such as k-means, neural networks, and feature-based indices (IC topography, spectral activity, ERPs, dipoles, event-related spectral perturbation, and intertrial coherence), among others, have been used in ICA clustering research (Contreras-Vidal & Kerick, 2004; Delorme et al., 2007; Huang, Jung, Delorme, & Makeig, 2008; Onton et al., 2005; Onton & Makeig, 2006; Onton, Westerfield, Townsend, & Makeig, 2006; Zeman, Till, Livingston, Tanaka, & Driessen, 2007). The common restriction of most of these algorithms resides in the need of an a priori determination of the number of IC clusters (ICc), which inherently entails the possibility that subjective bias could be introduced to the results (Onton & Makeig, 2006; Zeman et al., 2007). Several proposals have been made to automatically determine the number of clusters (see, e.g., Fraley & Raftery, 1998; Lange, Roth, Braun, & Buhmann, 2004; Martinez & Martinez, 2004; Still & Bialek, 2004, among many others), but their application of ICA to brain electrophysiological data has been scarce. In the present study, we used the model-based clustering (MBC) approach (Fraley & Raftery, 1998; Martinez & Martinez, 2004), based on the finite mixture model for probability densities, to calculate, in a nonsupervised way and without a priori assumptions regarding the number of clusters required as an input, the number of statistical ICcs that reliably contribute to the formation of an ERP. Our hypothesis is that if the MMN memory-based model is correct in claiming that MMN is a different process superimposed on N1, then we should be able to find ICs comprising standard and deviant responses in different clusters. In this model, a cluster or clusters should ideally contain standard N1 ICs, including some with the MMN ICs in their respective expected time ranges, and some common MMN/N1 ICs. If the adaptation model holds true, we should identify common ICs to standard and deviant-response N1 ICs in the same cluster(s), leading to the interpretation that N1 and MMN ERPs consist of a similar mechanism of brain dynamics.

## Materials and Methods

### Participants

Fifteen right-handed, healthy participants (7 women; mean age 25.4 years; range 20–28 years) gave their written consent to participate in the study. None of the participants reported a history of head injury, neurological disease, hearing problems, severe medical illness, or drug abuse. The experiment was approved by the Ethics Committee of the University of Barcelona.

### Stimuli and Procedure

The paradigm consisted of trains of three pure sine-wave tones (1000 Hz, 10-ms rise/fall times) delivered binaurally through headphones (90 dB SPL) by the Stim Interface System (Neuroscan Inc.). The first two tones (S1 and S2) were 75 ms in duration (standard tones), and the third tone was, in the same proportion ($P = .5$), either a standard ($N = 100$) or a deviant tone ($N = 100$) of 25 ms in duration.

The order of standard and deviant trains was random, the intrastimulus interval was 584 ms, and the intertrain interval was 30 s (Fuentemilla, Marco-Pallarés, & Grau, 2006). The MMN and neural oscillatory activity results using the same subjects and paradigm were described in a previous study (Fuentemilla, Marco-Pallarés, Münte, & Grau, 2008).

Participants sat in a comfortable chair in a dimly lit, electrically and acoustically shielded booth. During the EEG recording, each subject was instructed to perform an irrelevant visual task (reading), to ignore the auditory stimuli, and to avoid extra eye movements and blinking.

### EEG Recording

EEG activity (0.01–70 Hz band-pass; 50 Hz notch filtered) was recorded by a 32-channel amplifier (Synamps, Neuroscan, Inc.) at a sampling rate of 500 Hz. EEG electrodes were placed according to the enhanced 10-20 position system (Fp1/2, F3/4, C3/4, P3/4, F7/8, T3/4, T5/6, Fz, Cz, Pz, Oz, FC1/2, FT3/4, M1/2, IM1/2, TP3/4, CP1/2) and were all referenced to the tip of the nose. Impedances were maintained below 5 kΩ. Ocular movements (EOG) were recorded from two electrodes at the outer canthus of each eye. A single ground electrode was attached at AFz.

### Data Analysis

The ERP protocol analysis consisted of a sequence of five steps delineated in Figure 1 and explained in detail in the following paragraphs.

**ERP analysis.** For each subject, continuous EEG data were band-pass filtered offline (1–35 Hz). Only epoched trials of 550 ms (150 ms prestimulus to 400 ms poststimulus) containing responses to the third standard of the train or deviant were extracted. The mean EEG at each channel for each epoch, rather than the mean EEG in a prestimulus baseline, was removed to improve the number of reliable ICs (Groppe et al., 2009). Trials were excluded automatically if amplitudes exceeded ±100 μV in EEG and/or EOG. ERPs were found by separately averaging EEG epoch trials with standard or deviant tones, while the MMN difference wave was calculated by subtracting the averaged deviant ERP from the averaged standard ERP. For each participant, differences between deviant and standard conditions were assessed with a repeated measures, two-tailed cluster mass permutation test (family-wise corrected with an alpha of 0.05; Bullmore et al., 1999; Groppe, Urbach, & Kutas, 2011a) using a recent EEGLAB toolbox developed by David M. Groppe (http://openwetware.org/wiki/Mass_Univariate_ERP_Toolbox; Groppe, Urbach, & Kutas, 2011b). Points between 0 and 250 ms after stimuli onset and all electrodes were included in the test. Electrodes within 5.44 cm of one another were considered spatial neighbors. A total of 2,500 random permutations were used to compute the repeated measures $t$ test null hypothesis distribution.

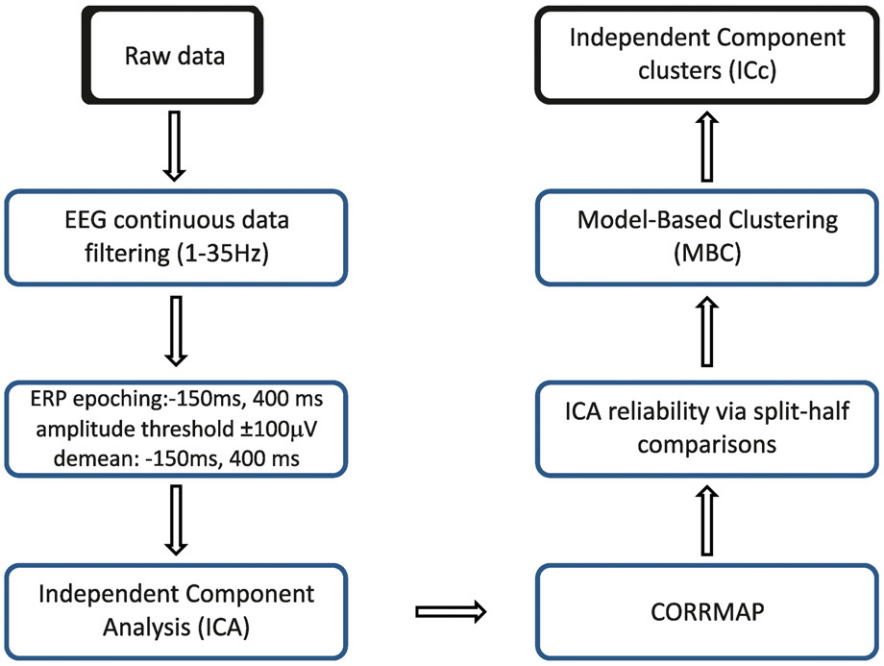


**Figure 1.** Data analysis steps. The initial and final data are in black squares, and the analysis steps are in blue squares.

**ICA.** The Infomax ICA algorithm finds the unmixing matrix, **W** (components by electrodes), which linearly decomposes an m-sensor EEG time series, **x**(t), into *n*-IC time series ($n \leq m$), **u**(t), where t represents each time point:

$$\mathbf{u}(t) = \mathbf{W}\mathbf{x}(t) \quad (1)$$

An IC is represented by two main features: the activation (rows of **u**(t) matrix) and the scalp topography (**A**, electrodes by components) corresponding to the inverse of the **W** unmixing matrix, as follows:

$$\mathbf{x}(t) = \mathbf{W}^{-1}\mathbf{u}(t) = \mathbf{A}\mathbf{u}(t) \quad (2)$$

whose columns define the weights of the projections of *n* IC to each scalp electrode. Because the polarity of the IC scalp map and activity are arbitrary, only their products determine the sign and the amplitude of each channel's potential (Onton & Makeig, 2006).

The extended Infomax algorithm (Lee, Girolami, & Sejnowski, 1999) was used for the ICA of the concatenated standard and deviant single-subject trials; that is, stimuli from both conditions were pooled to increase the robustness of the ICA decomposition (Groppe et al., 2009). IC extraction was performed with EEGLAB (v6.01b) software under MatLab 7.2, as described by Delorme and Makeig, 2004.

**ICA artifact rejection.** After ICA, CORRMAP was run in automatic mode to detect, in a semiautomatic way, which ICs enclosed eye blinks and lateral eye movements. First, a preselection of representative artifact templates was used to draw correlations between these templates and the ICs from all participants (Viola et al., 2009). In a second step, the remaining ICs were subjected to a visual inspection to identify nonstereotype artifacts (e.g., bad electrode contacts, muscular activity, etc.). The identification of such artifactual ICs was based on the scalp and time course characteristics (Jung et al., 2000, 2001).

**ICA reliability via split-half comparisons.** ICA reliability was assessed using the split-half approach (Groppe et al., 2009). This method determines the reliability of each subject's IC by splitting individual data into two halves (odd and even trials) and computing the distance of topography and activation features found in each half with those found when entering the whole dataset. To statistically test the reliability of a certain IC (in our case, that two ICs are homogeneous or not), a probabilistically interpretable reliability criterion was used (see Groppe et al., 2009, for details).

This analysis was performed for standard and deviant conditions together. The MatLab code for implementing the split-half reliability analysis is freely available at David M. Groppe's website (http://www.cogsci.ucsd.edu/~dgroppe/eeglab.html).

After the reliability analysis, ICs were inspected, and only those with (a) a minimum of 10 consecutive statistically significant samples in comparison with the mean of their baseline activity (−100 to 0 ms; repeated measures *t* test thresholded at $p < .05$); (b) a minimum contribution of 5% of the IC activation back-projected ERP variance (using "eeg_pvaf" EEGLAB function) during the poststimulus interval (0 ms to 400 ms after the onset of the stimulus), that is, the IC must have accounted for 5% of the MMN or N1 for that subject within this time window; and (c) showing topographies (i.e., frontocentral distribution at the scalp) and time activations (i.e., appearing 80 to 250 ms after the stimuli onset) compatible with the N1/MMN scalp distribution, were selected for further analysis.

**Independent component clustering.** To test whether different or similar ICs would result in response to standard and deviant tones across participants, we applied MBC because it requires no a priori knowledge of the number of clusters (Fraley & Raftery, 1998; Martinez & Martinez, 2004), and only the specification of the maximum number of clusters is required. MBC is based on the finite mixture model for probability densities (Martinez & Martinez, 2004), which assumes that the probability density function

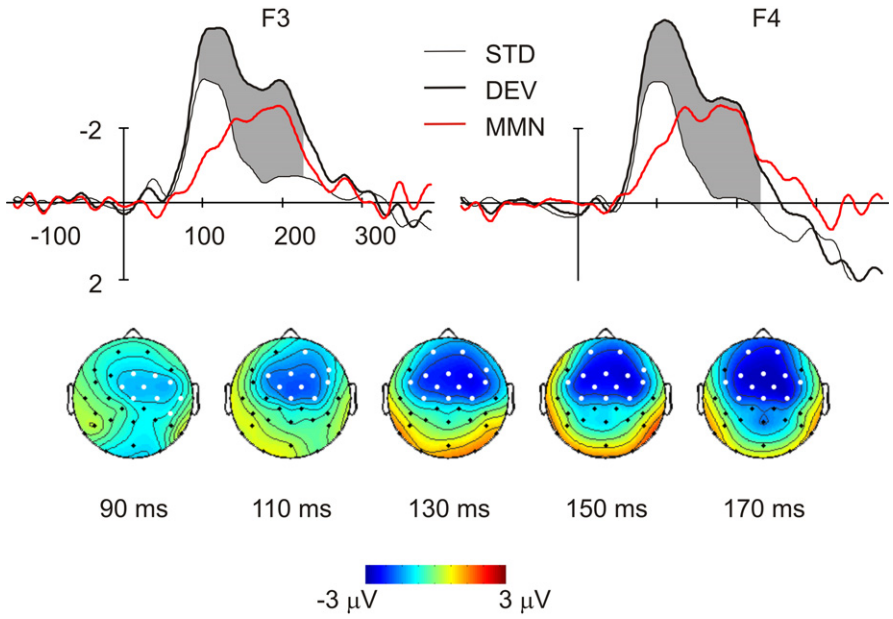


**Figure 2.** Top: Grand mean of the standard (thin gray line), deviant (thick black line), and MMN difference waves (thick red line). F4 presented significant differences ($p_{corrected} < .05$) from 78 ms to 240 ms after incoming stimuli, $t_{unc}$ (14) = 4.07, $p_{unc} = .001$, $d = 0.84$, while in F3, this difference was significant from 92 to 230 ms, $p_{corrected} < .05$; $t_{unc}$ (14) = 5.15, $p_{unc} = .0001$, $d = 1.07$). Bottom: Isovoltage significant cluster of electrodes (white electrodes; from −3 μV to 3 μV) topographic maps for the deviant versus standard comparison.

can be modeled as the sum of the weighted component densities, and if the covariance matrix is constrained with a model, the particular multivariate normal density data can be explained. The term *model* refers to the type of constraint applied to and the geometric properties of the covariance matrix. First, the algorithm implements the model-based agglomerative clustering, which provides an initial configuration of the maximum number of clusters. Next, the expectation-maximization algorithm refines the estimations obtained from the model-based agglomerative clustering. Finally, the Bayesian information criterion (BIC) is used to provide a measure of the appropriateness of a model and the number of clusters (Martinez & Martinez, 2004). The EDA Toolbox (http://lib.stat.cmu.edu/matlab/) was selected to implement the algorithm, and an in-house program (freely available at www.brainvitge.org/software.php) was created to integrate the MBC into EEGLAB clustering options. The maximum number of clusters allowed was set to 10. Previously, IC activation stimulus response 80–250 ms was selected as a clustering feature being reduced to 10 dimensions by principal component analysis. For each participant, differences between deviant and standard conditions were assessed with the $T_{max}$ permutation test (Blair & Karniski, 1993; Groppe et al., 2011a). All time points between 100 and 200 ms after the stimuli onset were used, and 2,500 random permutations of the data were used to estimate the distribution of the null hypothesis.

## Results

### ERPs

A total of 1,477 trials were obtained for the standard condition (98.5 ± 1.4 per subject, mean ± *SD*), and 1,382 for the deviant condition (98.7 ± 1.2). Significant differences were obtained between the deviant and standard response amplitudes within the MMN time range using the cluster permutation test. A first significant cluster was identified at the frontocentral scalp regions. Figure 2 shows the time evolution at the F3 and F4 electrodes for the deviant (thick black line), standard (thin black line), and the corresponding difference waveform (red line) between both conditions. F4 presented significant differences ($p_{corrected} < .05$) from 78 ms to 240 ms after stimuli onset, $t_{unc}$ (14) = 4.07, $p_{unc} = .001$, $d = 0.84$, and for F3, this difference was significant from 92 to 230 ms, $p_{corrected} < .05$; $t_{unc}$ (14) = 5.15, $p_{unc} = .0001$, $d = 1.07$. None of the mastoid electrodes showed significant differences between both conditions using the cluster permutation test.

### ICA and Reliability Via Split-Half Comparisons

After ICA, 30 ICs per participant were obtained (450 ICs in total). CORRMAP identified a total of 21 frontal ICs associated with eye blinks (mean correlation = 0.96; correlation threshold = 0.8) and 15 lateral eye-movement ICs (mean correlation = 0.97; correlation threshold = 0.85; Supplementary Figure 1) across the 15 participants. Then, split-half reliability analysis was applied by dividing the data into three separate datasets (odd trials, even trials, and all trials). All possible pairs of ICs from the full dataset and from each half of the data were formed, and those pairs presenting significant lower distance metrics in the joint distribution of the topography and activation distances were selected as reliable (see Groppe et al., 2009, for a more detailed description of the topography and activation distance metrics). After split-half reliability analysis, a total of 202 (55.11% IC rejection) reliable ICs were obtained (13.47 ± 4.12 per subject; mean ± standard deviation; see Supplementary Figure 2 for more details). The percentage of ICs that overcame the abovementioned criteria was remarkably similar to the original Groppe et al., 2009, study (for a direct comparison, see Figure 7, Experiments 3 and 4 of Groppe et al., 2009). ICs that survived reliability split-half analysis were submitted to a second threshold step explained in the ICA reliability via the split-half comparison

paragraph of the Methods section. As a result, a total of 60 ICs overcame (a) temporal activation, (b) variance explained, and (c) topography criteria. All participants contributed, with a minimum of 1 IC and a maximum of 7 ICs (see Supplementary Figure 3 for illustrative examples).

The present ICA reliability results (percentage of reliable ICs for 30 electrodes) are remarkably similar to the original study (Garrido et al., 2009). Of those, a total of 60 reliable ICs remained significant after the application, for each participant and IC, of the three criteria explained in the ICA reliability via split-half comparison paragraph of the Methods section (see above). All participants contributed, with a minimum of 1 IC and a maximum of 7 ICs (see Supplementary Figure 3 for illustrative examples).

Finally, to test the accuracy of the IC modelling of the N1 and MMN, we compared the signal-to-noise ratios (SNR) of the artifact-corrected data (after split-half reliability, CORRMAP, and visual inspection to identify nonstereotype artifacts) and the SNR from the ICs included in the three clusters. The SNR was computed by dividing the root mean square of each IC for each participant around the N1 (90–120 ms) and MMN (140–188 ms) peaks by the variance of their respective baselines (−150 to 0 ms). This analysis revealed that the SNRs of the artifact-corrected data and the ICs selected for cluster analysis were not significantly different for either the N1 ($t$ test; $p = .78$) or the MMN ($t$ test; $p = .81$) (Supplementary Figure 4). Thus, the IC modeling is not significantly different from the clean EEG data.

### Independent Component Clustering

The MBC found three ICcs (Figure 3, Supplementary Figure 5 for BIC curves). ICc1 included 29 ICs from 12 participants with frontocentral scalp distribution and right mastoid polarity inversion. ICc2 grouped 19 ICs from 10 participants, and ICc3 pooled 12 ICs from 10 participants. These clusters were also characterized by frontocentral topographies, with ICc2 more anterior than ICc3 (Figure 3).

In a second step, ERPs for the standard and deviant conditions were back-projected separately. As explained above, to increase the number of time points per channel, we decided to pool together the standard and deviant trials. As our main research question was to test whether the MMN was a modulated N1, we used the clustered spatial filters to calculate the standard and deviant activations separately. To avoid any ambiguity in the maps and activations in the scalp of the components (Onton & Makeig, 2006), the "std_comppol.m" EEGLAB function was used to find the polarity inversions (if any) of each IC from each ICc and each participant. Each IC scalp map activation magnitude was normalized by multiplying their root mean square amplitude using the "std_erp.m" EEGLAB function. ICc1 and ICc2 showed clear N1 responses for standard and deviant conditions, with no significant differences between the standard and deviant conditions. In addition to the N1, ICc3 showed significant differences ($p_{corr} < .05$) in the MMN time range using the $T_{max}$ permutation approach (110–136 ms; $t(9) = 4.43$, $p_{unc} = .002$, $d = 0.34$).

To further validate our approach, we considered the amount of variance explained by each of the three ICcs of the F3 and F4 electrodes. These electrodes were selected as representative of this analysis because they are the traditional electrode locations for which the MMN and N1 show maximal amplitudes and because they both showed significant differences between the deviant and standard conditions in our experiment. For each of the three ICcs, the amount of explained variance from the artifact-corrected ERPs was calculated separately for the standard and deviant conditions and the MMN contrast using the EEGLAB function "eeg_pvaf.m." ICc1 explained a mean of 41.78% and 45.43% of the standard and deviant ERP amplitude variances, respectively; ICc2 explained 44.89% of the standard and 49.28% of the deviant ERPs; and ICc3 explained 45.68% of the standard and 49.09% of the deviant ERP amplitude. In addition, ICc3, the unique cluster for which standard and deviant responses differed statistically, accounted for 90.23% of the MMN brain response computed with the classical difference wave approach.

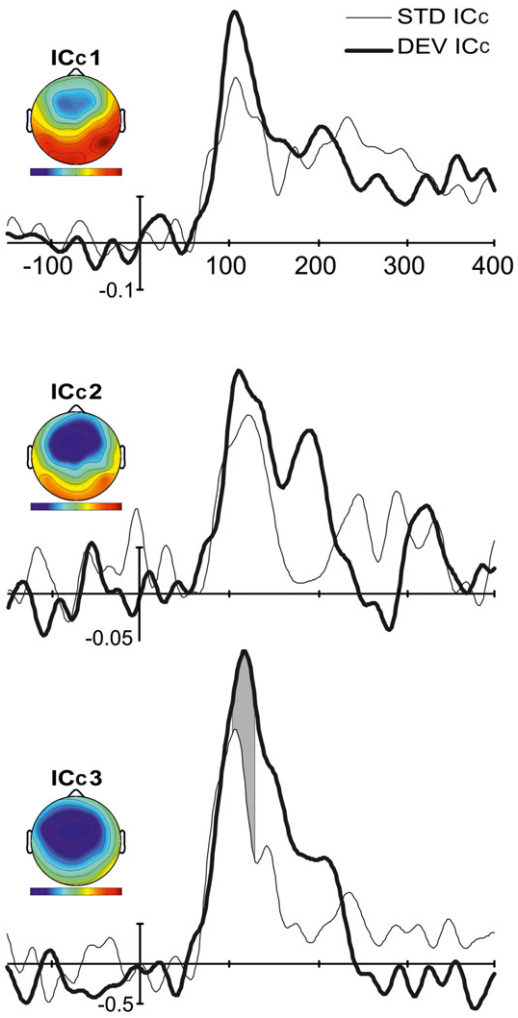


**Figure 3.** Clustering results. The MBC found 3 different clusters (ICc1, ICc2, and ICc3). Scalp topographies are normalized to the unit and averaged. ICc1 included 29 ICs from 12 participants with frontocentral scalp distribution and right mastoid polarity inversion. ICc2 grouped 19 ICs from 10 participants, and ICc3 pooled 12 ICs from 10 participants. Gray areas indicate statistically significant ($p_{corr} < .05$) time ranges using the $T_{max}$ permutation approach (110–136 ms; $t(9) = 4.43$, $p_{unc} = .002$, $d = 0.34$) from the deviant versus standard comparison. Note that because the IC scalp map and activity are arbitrary, only their product determines the sign and the amplitude of the potential of each activation time course.

### Discussion

We combined ICA and MBC to study whether the auditory EEG MMN and the N1 could be explained by a single or a dissociated component that is detectable at the scalp. Our approach combined

a split-half reliability ICA (Groppe et al., 2009) and an MBC analysis (Fraley & Raftery, 1998; Martinez & Martinez, 2004). The combination of the two procedures allowed us to filter out statistically nonrobust ICs and search for reliable ICs across participants without a priori information about the number of clusters. Our findings showed that most of the ICs identified across participants in response to standard and deviant auditory conditions were grouped in two clusters (ICc1 and ICc2), both located at the frontocentral scalp regions. Furthermore, these two clusters yielded indiscernible (nonsignificant) N1s for both standard and deviant sounds, with higher right mastoid activity for the former. Strikingly, we also found a third frontocentral cluster (ICc3) with significant differences in the MMN time range. Previous studies using ICA have shown that auditory N1s and MMNs could be decomposed into different ICs, which may be associated with different functional spatiotemporal neural dynamics of the brain auditory responses (Grau et al., 2007; Kalyakin et al., 2008; Makeig et al., 1997; Marco-Pallarés et al., 2005). However, the ICA protocols used in these studies were very different from those used here. None of these studies applied reliability or clustering analysis to the ICs, so there is no guarantee that the resulting ICs were stable within the experiment and across participants. Moreover, a previous MMN study from our group used a difference waveform approach in the ICA computation (Marco-Pallarés et al., 2005), which indirectly assumes that the N1 and MMN are different brain responses. In addition, and given that the goal of none of these studies was to evaluate competing theories about the MMN origin, the results shown in some of these studies analyzing MMN by means of ICA were only the difference waveform (Marco-Pallarés et al., 2005) or the deviant response (Kalyakin et al., 2008). These methodological limitations increased the difficulty in interpreting previous ICA results in light of both the memory-based and adaptation hypotheses.

Of the competing hypotheses of MMN generation, our results seem to fit better to the adaptation model rather than to the memory-based model. The adaptation model predicts that the MMN would be generated by a partially overlapping patch of neurons in the auditory cortex that respond to the deviant sound but, interestingly, also to the standard sound. The ICc1 and ICc2 data support this hypothesis, given that the ICc activations for the standard and deviant tones showed equivalent N1 ERPs. The adaptation model further argues that the differences in the response to the deviant and standard sounds would rely on the neurophysiological adaptation response caused by the auditory stimulation, with the neural activity to the entrance of a deviant sound being less adapted (i.e., less suppressed) than to a standard sound. Critically, this model predicts that the N1 and the MMN would involve activity from similar auditory brain areas, which confirms the conclusion that the MMN may constitute a mere modulation of the N1 component at the scalp (May & Tiitinen, 2010). This argument is further supported by our results because ICc3 showed a statistically significant enhancement of the deviant N1 in comparison with the standard N1.

In contrast, the memory-based hypothesis presumes the existence of a fundamental distinction between the N1 and the MMN. In accordance with this hypothesis, two neural systems can be differentiated in the auditory processing: the "transient detector system" and the "feature detector system." N1 would be related to the former by expressing the need to detect energy changes elicited by input stimuli; and MMN would analyze the physical features of incoming stimuli, comparing them with those engendered by previous auditory stimulation, consequently acting as a sensory memory comparison process (Näätänen, 1992). Hence, and critically for the interpretation of our results, these two systems would be identified as two separate components by the scalp EEG. The present data do not support this possibility because we failed to find any ICc that was uniquely contributed by ERP data that was elicited by the deviant stimuli but not by the standard sound. In addition, the current study showed that the MBC was also classified in a third ICc (ICc3) that presented significant differences between the standard and deviant conditions that are compatible with the existence of a dissociated N1 component, the N1a, which would correspond to the MMN time range (Jääskeläinen et al., 2004) and the N1p, appearing later in latency, which would be more suppressed in response to the deviant sound (Jääskeläinen et al., 2004).

Methodologically, we believe the approach presented here may open new horizons in the interpretation of other ERP components described in the literature. Traditional ERP analysis assumes that brain signal acquisition at the scalp is equivalent for all participants. This argument, however, does not take into account that infinite brain source configurations and individual neuroanatomical and neurophysiological differences might affect the electrical propagation of the same ERP component of the scalp sensor space (Baillet, Mosher, & Leahy, 2001). Across-participant IC clustering overcomes the questionable assumption that the sources for each participant are projected to the scalp in an equivalent way (Onton & Makeig, 2006; Onton et al., 2006). However, traditional clustering analysis (such as k-means or neural networks) requires a prior determination of the number of clusters to be extracted. To our knowledge, this is the first study that combined ICA and MBC in EEG research (see, however, Neumann, von Cramon, & Lohmann, 2008; Neumann, Fox, Turner, & Lohmann, 2010, for fMRI applications). MBC groups the IC features across participants and conditions without a priori assumptions about the number of clusters, the participants' identity, or the experimental condition. However, compared to the k-means, hierarchical clustering algorithms and all other approaches used in the abovementioned studies (such as in Contreras-Vidal & Kerick, 2004), MBC goes one step further and determines which statistical model (out of 9 possible models) fits better with a specific number of clusters (from 1 to a mandatory maxima, e.g., 10). Then, MBC systematically combines the information of the number of clusters in the data and the type of constraint that best explains them. With the unsupervised clustering analysis, it is possible to study the individual data and discover how robust and reproducible one particular experimental condition is across the whole sample of participants (Onton & Makeig, 2006; Onton et al., 2006).

A challenging option to consider with this unsupervised clustering approach is the comparison of ERP components from different experimental paradigms, following the rationale of the meta-analytic studies (Neumann et al., 2008, 2010). For example, it is argued that the MMN component in response to auditory changes in frequency, duration, intensity, gap, and location is generated in different regions of the auditory cortex; however, it is unclear to what degree neural mechanisms of sensory memory comparison or adaptation processes contribute to each of these factors (Näätänen et al., 2007). To solve this question, an ICA of the MMN ICs from different experiments (using frequency, duration, intensity, gap, and location deviants) with their respective samples of participants could be grouped using MBC analysis. In that way, one could answer experimental questions by not only comparing different conditions from the same/different participants, but also by comparing different conditions from different experiments using either the same or different participants.

It is worth mentioning some limitations of the current methodological approach. First, the split-half reliability analysis was performed on a relatively low number of trials (Groppe et al., 2009). The number of reliable ICs depends on the amount of training data, and it is possible that the conservative criteria hampered the survival of specific ICs, among these ICs, the "genuine" MMN component. Nevertheless, if this was the case, it would mean that the "genuine" MMN is less statistically robust than the N1, which is in agreement with some studies (Dalebout & Fox, 2001; Lew, Gray, & Poole, 2007; Martin & Boothroyd, 1999; Picton, Alain, Otten, Ritter, & Achim, 2000).

However, the main limitation of the present study is the modest spatial resolution (30 channels). In ICA, the successful demixing of different brain sources is determined by the number of electrodes and the number of time points per channel (Lee et al., 1999). It has been suggested that the spatial overlapping of different IC sources could be explained by the limited spatial resolution (implicitly constrained because of the low number of electrodes; Baillet et al., 2001). Consequently, it could be difficult to fully separate neighboring neural populations participating in distinct processing tasks or the contribution of intermixed neuronal populations located in the same brain structure that are performing different brain computation processes (Marco-Pallarés et al., 2005). Taking into account this previous evidence, we precluded ourselves from using dipoles or other source reconstruction algorithms whose outputs could have been used as a cluster feature in combination with the ERP ICs' activation time courses (Gramann et al., 2009; Onton et al., 2006). Further studies with different stimulation paradigms and higher dimensional data (64 or more electrodes) using the combined ICA-MBC must be performed to test if the number of ICcs changes.

Another limitation, due to the intrinsic data-driven property of the ICA, is that the split-half reliability analysis promotes the most reliable ICs across time and space that, in turn, may have been affected by EEG noise or artifacts common during an experimental setting or when, for example, EEG data are obtained from common artifacted electrodes from different participants across the same experiment. This may lead to increasing the cut-off values of the critical region, occluding ICs with meaningful physiological interpretation. The introduction of criteria to identify and reject these ICs (e.g., by changing the cut-off of the values of the critical region, introducing new methods for automatic artifact rejection, such as the ADJUST plug-in (Mognon, Jovicich, Bruzzone, & Buiatti, 2011), or introducing new reliability methods may help solve this issue. In addition, it is important to note that, while the ICs that are included in the cluster analysis are reliable, there is no evidence that the clustering result found is reliable. This is a common limitation of several studies based on clustering that is based on ICA, and although there are already some procedures in use (see, e.g., Lange et al., 2004), data cluster estimation, comparison, and reliability assessment is an area of research itself beyond the scope of the present investigation. Finally, a possible caveat of MBC might be a lack of sensitivity to the type of constraints of the covariance matrix from the different models.

In conclusion, in the present study, we combined ICA and MBC, and we showed that EEG modulations in response to auditory standards and deviants can be explained by three frontocentral ICcs. These results lend support to the hypothesis derived from the adaptation model of MMN generation, which predicts that MMN represents the modulation of neural responses that are also associated with auditory N1.

## References


Alain, C., Woods, D. L., & Ogawa, K. H. (1994). Brain indices of automatic pattern processing. *Neuroreport*, *6*, 140–144.

Alho, K. (1995). Cerebral generators of mismatch negativity (MMN) and its magnetic counterpart (MMNm) elicited by sound changes. *Ear and Hearing*, *16*, 38–51.

Alho, K., Winkler, I., Escera, C., Huotilainen, M., Virtanen, J., Jääskeläinen, I., . . . Ilmoniemi, R. (1998). Processing of novel sounds and frequency changes in the human auditory cortex: Magnetoencephalographic recordings. *Psychophysiology*, *35*, 211–224. doi: 10.1111/1469-8986.3520211

Baillet, S., Mosher, J. C., & Leahy, R. M. (2001). Electromagnetic brain mapping. *Signal Processing Magazine, IEEE*, *18*, 14–30.

Blair, R., & Karniski, W. (1993). An alternative method for significance testing of waveform difference potentials. *Psychophysiology*, *30*, 518–524. doi: 10.1111/j.1469-8986.1993.tb02075.x

Bullmore, E. T., Suckling, J., Overmeyer, S., Rabe-Hesketh, S., Taylor, E., & Brammer, M. J. (1999). Global, voxel, and cluster tests, by theory and permutation, for a difference between two groups of structural MR images of the brain. *IEEE Transactions on Medical Imaging*, *18*, 32–42. doi: 10.1109/42.750253

Contreras-Vidal, J. L., & Kerick, S. E. (2004). Independent component analysis of dynamic brain responses during visuomotor adaptation. *Neuroimage*, *21*, 936–945. doi: 10.1016/j.neuroimage.2003.10.037

Dalebout, S. D., & Fox, L. G. (2001). Reliability of the mismatch negativity in the responses of individual listeners. *Journal of the American Academy of Audiology*, *12*, 245–253.

Debener, S., Makeig, S., Delorme, A., & Engel, A. K. (2005). What is novel in the novelty oddball paradigm? Functional significance of the novelty P3 event-related potential as revealed by independent component analysis. *Cognitive Brain Research*, *22*, 309–321. doi: 10.1016/j.cogbrainres.2004.09.006

Delorme, A., & Makeig, S. (2004). EEGLAB: An open source toolbox for analysis of single-trial EEG dynamics including independent component analysis. *Journal of Neuroscience Methods*, *134*, 9–21. doi: 10.1016/j.jneumeth.2003.10.009

Delorme, A., Westerfield, M., & Makeig, S. (2007). Medial prefrontal theta bursts precede rapid motor responses during visual selective attention. *The Journal of Neuroscience*, *27*, 11949–11959. doi: 10.1523/jneurosci.3477-07.2007

Deouell, L., Bentin, S., & Giard, M.-H. (1998). Mismatch negativity in dichotic listening: Evidence for interhemispheric differences and multiple generators. *Psychophysiology*, *35*, 355–365. doi: 10.1111/1469-8986.3540355

Fraley, C., & Raftery, A. E. (1998). How many clusters? Which clustering method? Answers via model-based cluster analysis. *The Computer Journal*, *41*, 578–588. doi: 10.1093/comjnl/41.8.578

Fuentemilla, L., Marco-Pallarés, J., & Grau, C. (2006). Modulation of the spectral power and of phase resetting of EEG contributes differentially to the generation of auditory event-related potentials. *Neuroimage*, *30*, 909–916. doi: 10.1016/j.neuroimage.2005.10.036

Fuentemilla, L., Marco-Pallarés, J., Münte, T. F., & Grau, C. (2008). Theta EEG oscillatory activity and auditory change detection. *Brain Research*, *1220*, 93–101. doi: 10.1016/j.brainres.2007.07.079

Garrido, M. I., Kilner, J. M., Stephan, K. E., & Friston, K. J. (2009). The mismatch negativity: A review of underlying mechanisms. *Clinical Neurophysiology*, *120*, 453–463. doi: 10.1016/j.clinph.2008.11.029

Giard, M.-H., Perrin, F., Pernier, J., & Bouchet, P. (1990). Brain generators implicated in the processing of auditory stimulus deviance: A topographic event-related potential study. *Psychophysiology*, *27*, 627–640. doi: 10.1111/j.1469-8986.1990.tb03184.x

Gramann, K., Onton, J., Riccobon, D., Mueller, H., Bardins, S., & Makeig, S. (2009). Human brain dynamics accompanying use of egocentric and allocentric reference frames during navigation. *Journal of Cognitive Neuroscience*, *22*, 2836–2849. doi: 10.1162/jocn.2009.21369

Grau, C., Fuentemilla, L., & Marco-Pallarés, J. (2007). Functional neural dynamics underlying auditory event-related N1 and N1 suppression

response. *Neuroimage*, *36*, 522–531. doi: 10.1016/j.neuroimage.2007.03.027

Groppe, D., Urbach, T., & Kutas, M. (2011a). Mass univariate analysis of event-related brain potentials/fields I: A critical tutorial review. *Psychophysiology*, *48*, 1711–1725. doi: 10.1111/j.1469-8986.2011.01273.x

Groppe, D., Urbach, T., & Kutas, M. (2011b). Mass univariate analysis of event-related brain potentials/fields II: Simulation studies. *Psychophysiology*, *48*, 1726–1737. doi: 10.1111/j.1469-8986.2011.01272.x

Groppe, D. M., Makeig, S., & Kutas, M. (2009). Identifying reliable independent components via split-half comparisons. *Neuroimage*, *45*, 1199–1211. doi: 10.1016/j.neuroimage.2008.12.038

Huang, R.-S., Jung, T.-P., Delorme, A., & Makeig, S. (2008). Tonic and phasic electroencephalographic dynamics during continuous compensatory tracking. *Neuroimage*, *39*, 1896–1909. doi: 10.1016/j.neuroimage.2007.10.036

Jääskeläinen, I. P., Ahveninen, J., Bonmassar, G., Dale, A. M., Ilmoniemi, R. J., Levänen, S., . . . Belliveau, J. W. (2004). Human posterior auditory cortex gates novel sounds to consciousness. *Proceedings of the National Academy of Sciences of the United States of America*, *101*, 6809–6814. doi: 10.1073/pnas.0303760101

Jung, T.-P., Makeig, S., Humphries, C., Lee, T.-W., McKeown, M. J., Iragui, V., & Sejnowski, T. J. (2000). Removing electroencephalographic artifacts by blind source separation. *Psychophysiology*, *37*, 163–178. doi: 10.1111/1469-8986.3720163

Jung, T.-P., Makeig, S., Westerfield, M., Townsend, J., Courchesne, E., & Sejnowski, T. J. (2001). Analysis and visualization of single-trial event-related potentials. *Human Brain Mapping*, *14*, 166–185. doi: 10.1002/hbm.1050

Kalyakin, I., González, N., Kärkkäinen, T., & Lyytinen, H. (2008). Independent component analysis on the mismatch negativity in an uninterrupted sound paradigm. *Journal of Neuroscience Methods*, *174*, 301–312. doi: 10.1016/j.jneumeth.2008.07.012

Kropotov, J., Alho, K., Näätänen, R., Ponomarev, V., Kropotova, O., Anichkov, A., & Nechaev, V. (2000). Human auditory-cortex mechanisms of preattentive sound discrimination. *Neuroscience Letters*, *280*, 87–90. doi: 10.1016/s0304-3940(00)00765-5

Lange, T., Roth, V., Braun, M. L., & Buhmann, J. M. (2004). Stability-based validation of clustering solutions. *Neural Computation*, *16*, 1299–1323. doi: 10.1162/089976604773717621

Lee, T.-W., Girolami, M., & Sejnowski, T. J. (1999). Independent component analysis using an extended infomax algorithm for mixed sub-Gaussian and super-Gaussian sources. *Neural Computation*, *11*, 417–441. doi: 10.1162/089976699300016719

Lew, H. L., Gray, M., & Poole, J. H. (2007). Temporal stability of auditory event-related potentials in healthy individuals and patients with traumatic brain injury. *Journal of Clinical Neurophysiology*, *24*, 392–397 doi: 310.1097/WNP.1090b1013e31814a31856e31813

Makeig, S., Bell, A. J., Jung, T.-P., & Sejnowski, T. J. (1996). Independent component analysis of electroencephalographic data. In M. M. D. Touretzky & M. Hasselmo (Eds.), *Advances in neural information processing systems* (vol. 8, pp. 145–155). Cambridge, MA: MIT Press.

Makeig, S., Debener, S., Onton, J., & Delorme, A. (2004). Mining event-related brain dynamics. *Trends in Cognitive Sciences*, *8*, 204–210. doi: 10.1016/j.tics.2004.03.008

Makeig, S., Jung, T.-P., Bell, A. J., Ghahremani, D., & Sejnowski, T. J. (1997). Blind separation of auditory event-related brain responses into independent components. *Proceedings of the National Academy of Sciences*, *94*, 10979–10984. doi: 10.1073/pnas.94.20.10979

Marco-Pallarés, J., Grau, C., & Ruffini, G. (2005). Combined ICA-LORETA analysis of mismatch negativity. *Neuroimage*, *25*, 471–477. doi: 10.1016/j.neuroimage.2004.11.028

Martin, B. A., & Boothroyd, A. (1999). Cortical, auditory, event-related potentials in response to periodic and aperiodic stimuli with the same spectral envelope. *Ear and Hearing*, *20*, 33–44.

Martinez, W. L., & Martinez, A. R. (2004). *Exploratory data analysis with MatLab 29*. Boca Raton, FL: CRC Press.

May, P., Tiitinen, H., Ilmoniemi, R. J., Nyman, G., Taylor, J. G., & Näätänen, R. (1999). Frequency change detection in human auditory cortex. *Journal of Computational Neuroscience*, *6*, 99–120. doi: 10.1023/a:1008896417606

May, P. J. C., & Tiitinen, H. (2010). Mismatch negativity (MMN), the deviance-elicited auditory deflection, explained. *Psychophysiology*, *47*, 66–122. doi: 10.1111/j.1469-8986.2009.00856.x

Mognon, A., Jovicich, J., Bruzzone, L., & Buiatti, M. (2011). ADJUST: An automatic EEG artifact detector based on the joint use of spatial and temporal features. *Psychophysiology*, *48*, 229–240. doi: 10.1111/j.1469-8986.2010.01061.x

Näätänen, R. (1992). *Attention and brain function*. Hillsdale, NJ: Lawrence Erlbaum.

Näätänen, R., Gaillard, A. W. K., & Mäntysalo, S. (1978). Early selective-attention effect on evoked potential reinterpreted. *Acta Psychologica*, *42*, 313–329. doi: 10.1016/0001-6918(78)90006-9

Näätänen, R., Jacobsen, T., & Winkler, I. (2005). Memory-based or afferent processes in mismatch negativity (MMN): A review of the evidence. *Psychophysiology*, *42*, 25–32. doi: 10.1111/j.1469-8986.2005.00256.x

Näätänen, R., Paavilainen, P., Rinne, T., & Alho, K. (2007). The mismatch negativity (MMN) in basic research of central auditory processing: A review. *Clinical Neurophysiology*, *118*, 2544–2590. doi: 10.1016/j.clinph.2007.04.026

Näätänen, R., & Picton, T. (1987). The N1 wave of the human electric and magnetic response to sound: A review and an analysis of the component structure. *Psychophysiology*, *24*, 375–425. doi: 10.1111/j.1469-8986.1987.tb00311.x

Näätänen, R., Tervaniemi, M., Sussman, E., Paavilainen, P., & Winkler, I. (2001). 'Primitive intelligence' in the auditory cortex. *Trends in Neurosciences*, *24*, 283–288. doi: 10.1016/s0166-2236(00)01790-2

Näätänen, R., & Winkler, I. (1999). The concept of auditory stimulus representation in cognitive neuroscience. *Psychological Bulletin*, *125*, 826–859. doi: 10.1037/0033-2909.125.6.826

Neumann, J., Fox, P. T., Turner, R., & Lohmann, G. (2010). Learning partially directed functional networks from meta-analysis imaging data. *Neuroimage*, *49*, 1372–1384. doi: 10.1016/j.neuroimage.2009.09.056

Neumann, J., von Cramon, D. Y., & Lohmann, G. (2008). Model-based clustering of meta-analytic functional imaging data. *Human Brain Mapping*, *29*, 177–192. doi: 10.1002/hbm.20380

Onton, J., Delorme, A., & Makeig, S. (2005). Frontal midline EEG dynamics during working memory. *Neuroimage*, *27*, 341–356. doi: 10.1016/j.neuroimage.2005.04.014

Onton, J., & Makeig, S. (2006). Information-based modeling of event-related brain dynamics. In N. Christa & K. Wolfgang (Eds.), *Progress in brain research* (vol. 159, pp. 99–120). Amsterdam, The Netherlands: Elsevier.

Onton, J., Westerfield, M., Townsend, J., & Makeig, S. (2006). Imaging human EEG dynamics using independent component analysis. *Neuroscience & Biobehavioral Reviews*, *30*, 808–822. doi: 10.1016/j.neubiorev.2006.06.007

Paavilainen, P., Alho, K., Reinikainen, K., Sams, M., & Näätänen, R. (1991). Right hemisphere dominance of different mismatch negativities. *Electroencephalography and Clinical Neurophysiology*, *78*, 466–479. doi: 10.1016/0013-4694(91)90064-b

Paavilainen, P., Simola, J., Jaramillo, M., Näätänen, R., & Winkler, I. (2001). Preattentive extraction of abstract feature conjunctions from auditory stimulation as reflected by the mismatch negativity (MMN). *Psychophysiology*, *38*, 359–365. doi: 10.1111/1469-8986.3820359

Picton, T. W., Alain, C., Otten, L., Ritter, W., & Achim, A. (2000). Mismatch negativity: Different water in the same river. *Audiology & Neuro-otology*, *5*, 111–139. doi: 10.1159/000013875

Still, S., & Bialek, W. (2004). How many clusters? An information-theoretic perspective. *Neural Computation*, *16*, 2483–2506. doi: 10.1162/0899766042321751

Tervaniemi, M., Saarinen, J., Paavilainen, P., Danilova, N., & Näätänen, R. (1994). Temporal integration of auditory information in sensory memory as reflected by the mismatch negativity. *Biological Psychology*, *38*, 157–167. doi: 10.1016/0301-0511(94)90036-1

Viola, F., Thorne, J., Edmonds, B., Schneider, T., Eichele, T., & Debener, S. (2009). Semi-automatic identification of independent components representing EEG artifact. *Clinical Neurophysiology*, *120*, 868–877. doi: 10.1016/j.clinph.2009.01.015

Yabe, H., Tervaniemi, M., Reinikainen, K., & Näätänen, R. (1997). Temporal window of integration revealed by MMN to sound omission. *Neuroreport*, *8*, 1971–1974.

Zeman, P. M., Till, B. C., Livingston, N. J., Tanaka, J. W., & Driessen, P. F. (2007). Independent component analysis and clustering improve signal-to-noise ratio for statistical analysis of event-related potentials. *Clinical Neurophysiology*, *118*, 2591–2604. doi: 10.1016/j.clinph.2007.09.001

(Received June 29, 2011; Accepted July 5, 2012)

**Supporting Information**

Additional supporting information may be found in the online version of this article:

**Figure S1:** CORRMAP results for blink and lateral eye movement artifacts.
**Figure S2:** Histograms of topography and activation distances for all possible IC pairs for the ICs from the standard plus deviant trials.
**Figure S3:** Examples of ERP images of the single trials of visual selected ICs submitted to MBC analysis from different participants and ICs.
**Figure S4:** SNR for N1and MMN peaks from artifact-corrected data and ICs selected to the cluster analysis.
**Figure S5:** BIC curves from the MBC analysis of the IC activations from the 60 ICs.

# Supplementary Figures

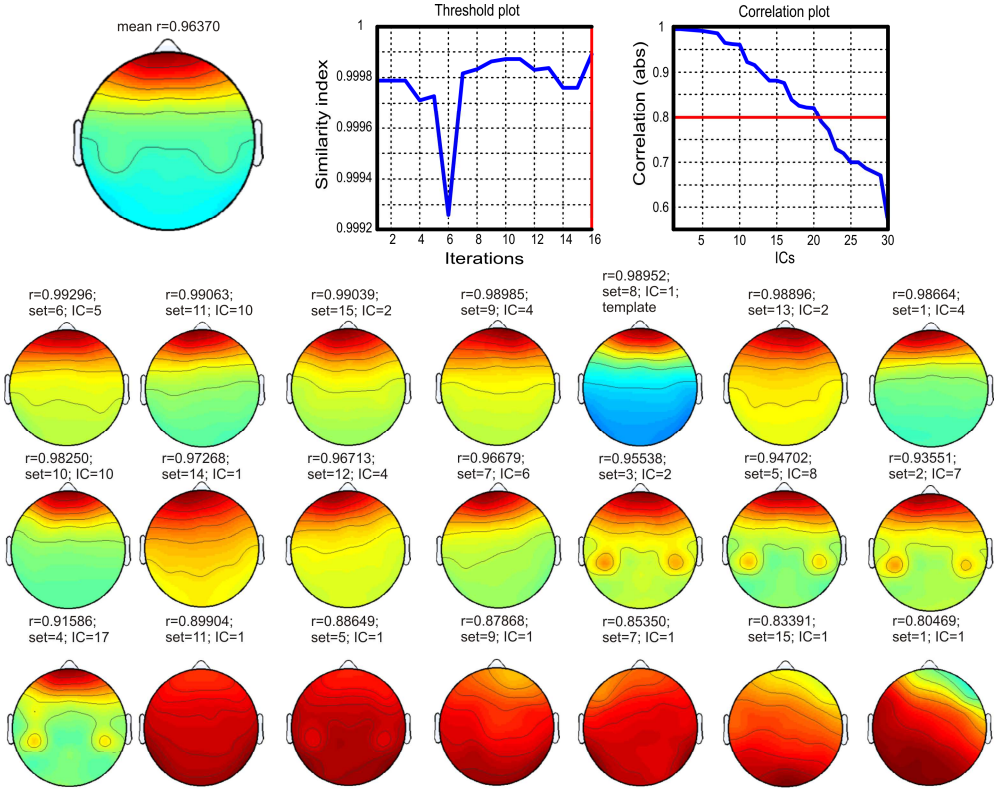


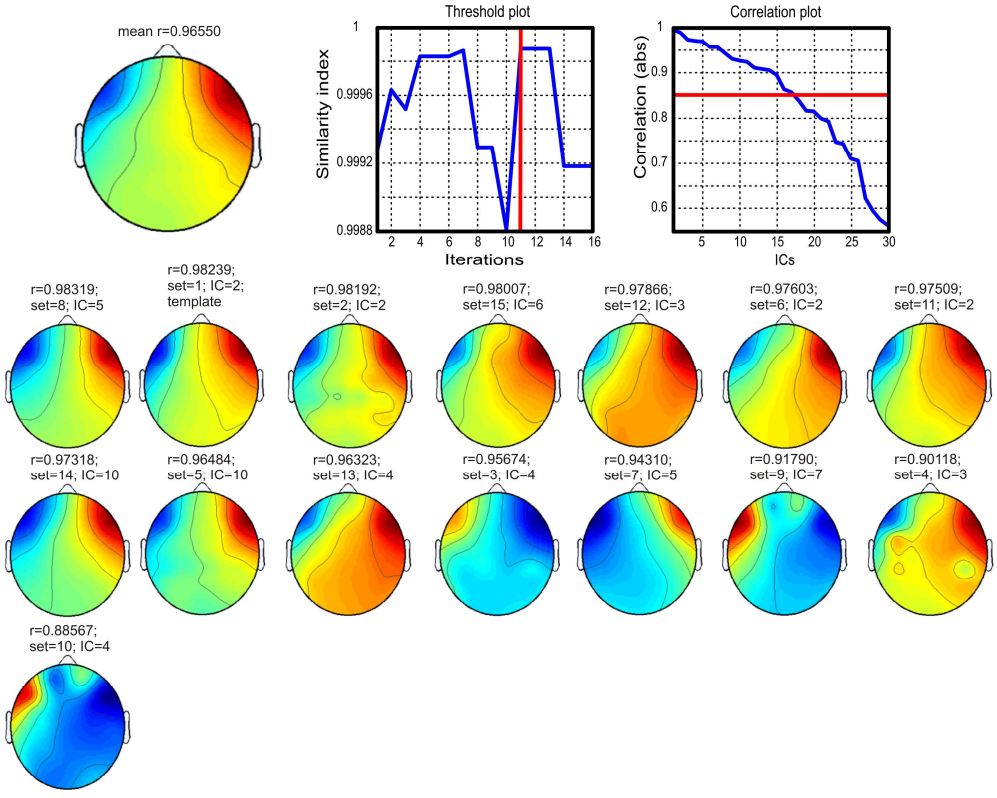

Supplementary Figure 1. CORRMAP results for blink (top) and lateral eye movement (bottom) artifacts. CORRMAP was run in automatic mode selecting a restriction of maximum of 2 ICs per dataset. CORRMAP found 21 frontal IC eyeblinks from the 15 participants (mean correlation = 0.96; correlation threshold = 0.8) and 15 lateral eye-movements ICs from 15 participants (mean correlation = 0.97; correlation threshold = 0.85).

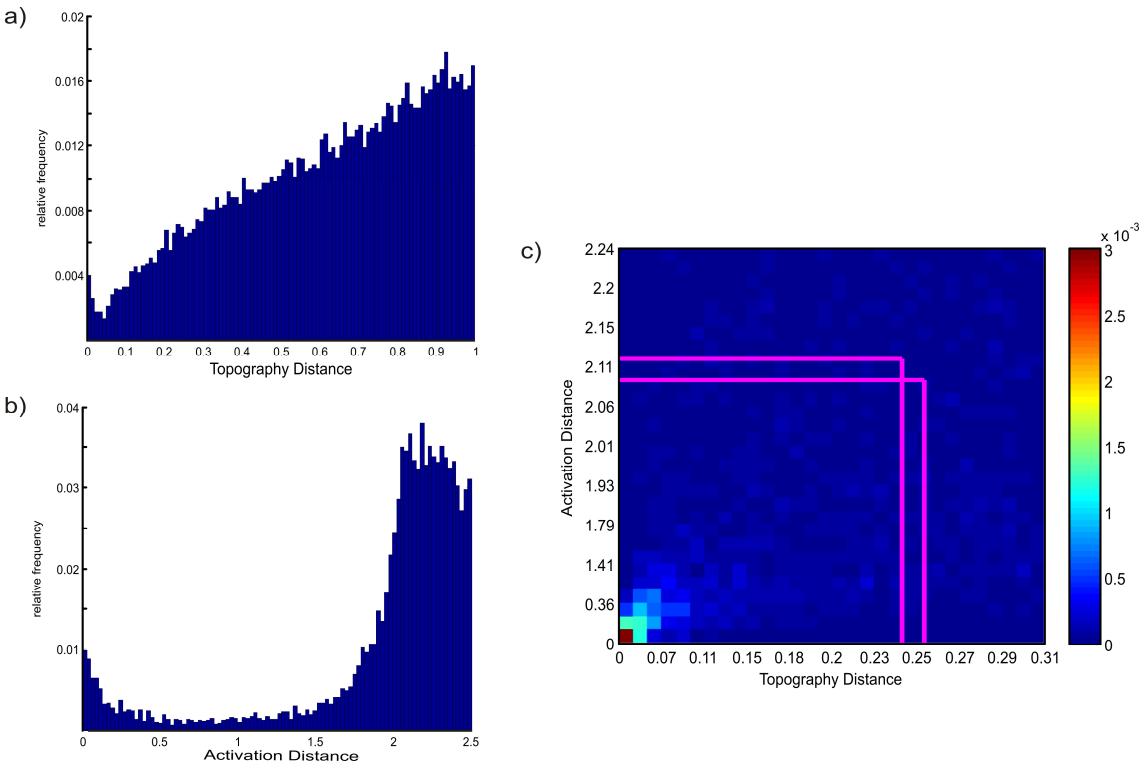


Supplementary Figure 2. Left) Histograms of topography and activation distances for all possible IC pairs for the ICs resulted from the standard plus deviant trials. Activation distance distributions were cut at 2.5, but the values tend toward infinite (data not shown). Relative histograms are derived from 40,500 IC pairs (i.e., 15 participants, 3 ICA decompositions per participant, 30 ICs per decomposition). Right) Joint distributions of IC pair topography and activation distances for all possible IC pairs for standard plus deviant trials. To make the two distance measurements comparable, they are binned in 5% increments. The distribution continues to the right and up (data not shown). Pink rectangles indicate the L-shaped critical region that contains 1/30 of all samples. The horizontal edge of the L-shaped critical region in the split-half comparison procedure as proposed by Groppe et al 2009 (the 10$^{th}$ percentile of the $dist_{topo}$ empirical distribution) was 0.2422 and the vertical (the $dist_{act}$ empirical distribution) was 2.1141. The second L-shaped region was 2.0927 (10$^{th}$ percentile of the $dist_{act}$ empirical distribution), and the other was 0.2543. Colorbar indicates relative frequency.

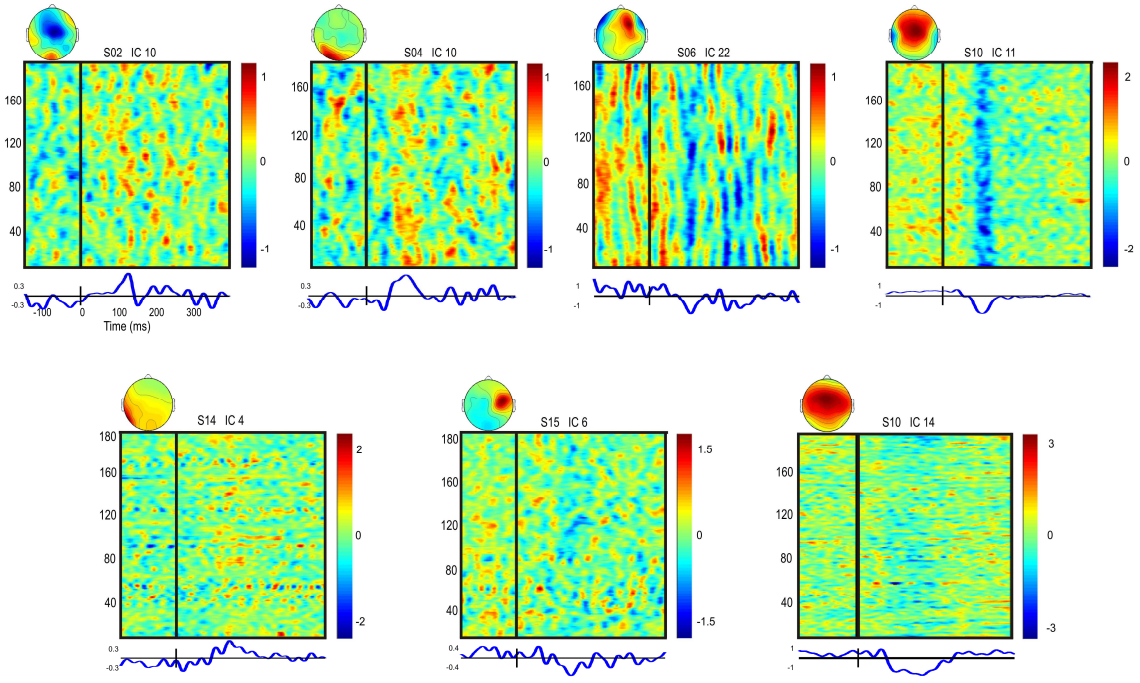


Supplementary Figure 3. Examples of ERPimages of the single trials (y axes, color coded as a single horizontal lines) of visual selected ICs submitted to MBC analysis from different participants and ICs. The bottom time course indicates the mean ERP IC activations of standard plus deviant trials. Time zero corresponds to the stimulus onset.

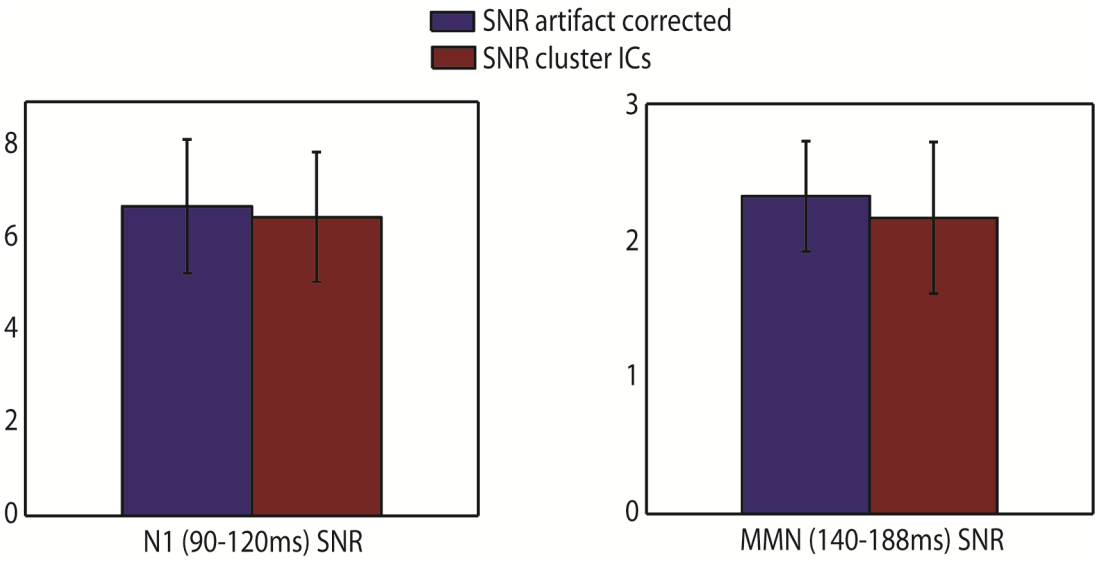


Supplemental Figure 4. SNR for N1 (90-120ms) and MMN (140-188ms) peaks from artefact corrected data (dark blue) and ICs selected to the cluster analysis (dark red). SNR was calculated dividing the mean root square of each IC activity for each participant around by the variance of their respective baselines (−100 to 0 ms).

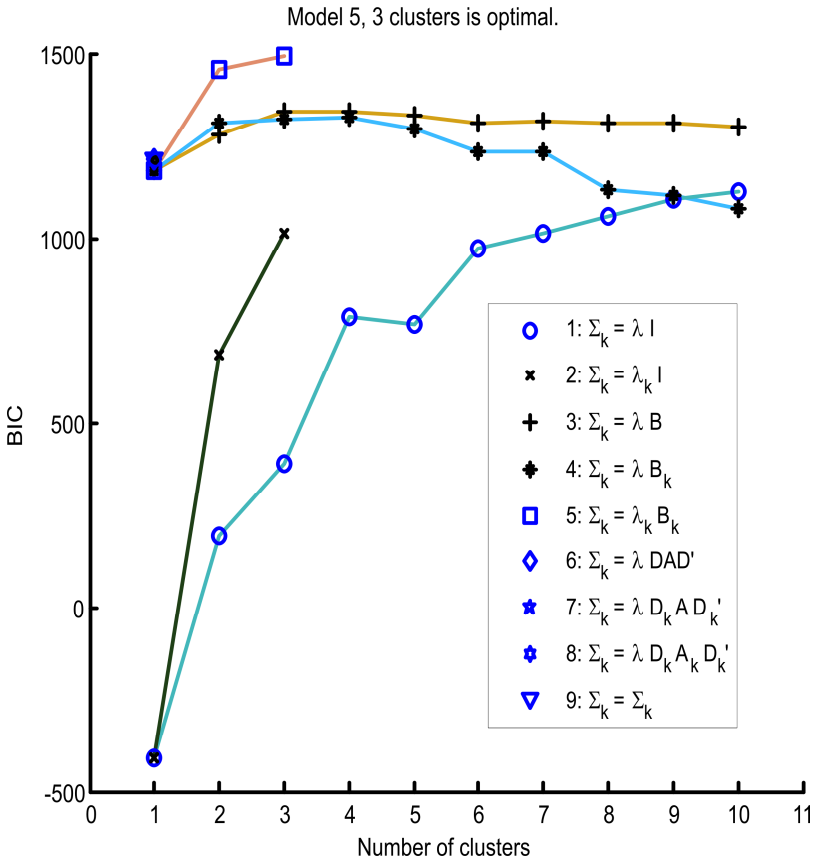


Supplemental Figure 5. Bayesian information criterion (BIC) curves from the MBC analysis of the IC activations from the 60 ICs. The maximum number of clusters was set to 10. Model 5 best explained the data, and the best fitted number of clusters is 3.